Title: Contrail properties over the eastern North Pacific from AVHRR data

Corresponding author: Patrick Minnis p.minnis@nasa.gov

Institution: Atmospheric Sciences, NASA Langley Research Center

Mailing address MS 420
NASA Langley Research Center
Hampton, VA 23681-2199 USA

Second author: Rabindra Palikonda r.palikonda@larc.nasa.gov
Third author: Bryan J. Walter b.j.walter@larc.nas.gov
Fourth author: J. Kirk Ayers j.k.ayers@larc.nasa.gov
Fifth author: Hermann Mannstein hermann.mannstein@dlr.de

Institution: AS&M, Inc., Hampton, VA 23666 USA

Contrail properties over the eastern North Pacific from AVHRR data

Patrick Minnis
Atmospheric Sciences, NASA Langley Research Center, Hampton, Virginia, USA
Rabindra Palikonda, Bryan J. Walter, J. Kirk Ayers
AS&M, Inc., Hampton, Virginia, USA
Hermann Mannstein
DLR Institut für Physik der Atmosphäre, Oberpfaffenhofen, Wessling, Germany

Abstract

An increase of air traffic over the North Pacific during the last 30 years has been accompanied by an increase in cirrus coverage. To help alleviate the uncertainty in the contribution of air traffic to the cirrus increase, an analysis of linear contrail coverage over the region has been initiated using afternoon *NOAA-16* AVHRR data taken during 4 months in 2002 and 2003. Manual evaluation of the automated contrail detection method revealed that it misclassified, on average, 32% of the contrail pixels as contrails and missed 15% of the contrail pixels. After correction for detection errors, the contrail coverage over the domain between 25° and 55°N and between 120° and 150°W varied from a minimum of 0.37% in February to a maximum of 0.56% in May, respectively. The annual mean coverage, after correcting for the diurnal cycle of air traffic, is 0.31%, a value very close to earlier theoretical estimates for the region. Contrail optical depths for the 4 months average 0.24 resulting in a mean unit contrail longwave radiative forcing of 14.2 Wm^{-2}. The contrail optical depths are twice the mean value expected from theoretical estimates.

Zusammenfassung

Der Zuwachs des Flugverkehrs über dem Nord-Pazifik während der letzten 30 Jahre ging einher mit einem Zuwachs der Zirrusbewölkung. Um die Unsicherheit in der Zuordnung dieses Zuwachses der Zirrusbewölkung zum Flugverkehr zu verringen, wurde eine Analyse der linearen Kondensstreifen

aus den AVHRR Daten der Nachmittagsüberflüge von NOAA-16 in 4 Monaten der Jahre 2002 und 2003 durchgeführt. Die visuelle Bewertung der automatischen Kondensstreifenerkennung ergab, dass 32% der erkannten Pixel zu Kondensstreifen gehörten, während 15% der Kondensstreifenpixel nicht erkannt wurden. Nach Korrektur dieser Erkennungsfehler ergab sich für das Gebiet zwischen 25° und 55°N und 120° und 150°W ein Bedeckungsgrad zwischen 0.36% im November und 0.56% im May. Der mit dem Tagesgang des Flugverkehrs korrigierte Jahremittelwert ist 0.31% und liegt somit nahe bei früheren, theoretisch ermittelten Werten für dieses Gebiet. Als mittlere otische Dicke wurde für diese 4 Monate der Wert 0.24 ermittelt, der einem mittleren Strahlungsantrieb im Infrarotbereich von 14.2 Wm^{-2} entspricht. Die optische Dicke ist doppelt so hoch, wie aus theoretischen Berechnungen erwartet.

1 Introduction

Cirrus cloud cover has been increasing over the North Pacific since the 1970's. Although part of the increase may be due to a rise in relative humidity, some of the change is likely caused by contrails forming and spreading as a result of transoceanic air traffic (e.g., ZEREFOS ET AL. 2003). Analysis of high-resolution satellite data is required to determine the contribution by linear contrails to that increase. The air traffic passes through a region where mean cirrus cloud coverage is generally about half that observed over land, while the upper tropospheric humidity, as indicated by the NCEP reanalysis at 300 hPa, is roughly 10% greater than that over land (MINNIS ET AL. 2004). Thus, the atmosphere over pristine oceanic regions should be more susceptible to contrail-cirrus cloud initiation than that over land areas. Additionally, transoceanic flights travel greater lengths at high altitudes than their continental counterparts and, therefore, should tend to produce longer contrails. The expected average linear contrail coverage from theoretical considerations for 1992 air traffic

[1] *Corresponding author:* Patrick Minnis, MS 420, NASA Langley Research Center, Hampton, VA, USA 23681. Email: p.minnis@nasa.gov

(SAUSEN ET AL. 1998) varies between 0% in the mid-Pacific and 1% near San Francisco Bay (Fig. 1a). The nominal flight corridors are well defined by the theoretical contrail coverage in Figure 1a; those in the eastern half of the domain are very similar to those seen in the more recent flight dataset of GARBER ET AL. (2004), which only includes flights east of 135°W. Fractional cirrus coverage rose between 0 and 0.006/year between 1971 and 1996 (MINNIS ET AL. 2004) over the same area, with a maximum increase over northern California (Fig. 1b). Over the ocean, a broad area with the greatest trends in cirrus coverage is centered near 45°N at the western edge of the domain in Figure 1. There is no obvious correlation between the cirrus trends and the theoretically derived contrail coverage. Understanding how the contrails actually, rather than theoretically, relate to the changes in cirrus coverage necessitates the development of some empirical data on the linear contrail coverage. To begin that effort, this paper presents analyses of contrail properties as derived from satellite data over the North Pacific. The retrievals are compared to similar quantities derived from data over the continental United States of America (USA) and other areas to examine the differences between contrails formed over marine and continental areas. They are also compared to the theoretical results to help understand the accuracy of models for predicting persistent contrails over the North Pacific.

2 Data and analysis

The 1-km window channel data from the Advanced Very High Resolution Radiometer (AVHRR) on the *NOAA-16* satellite are analyzed here using an automated detection method. Figure 2 shows examples of large contrails evident in the *NOAA-16* AVHRR imagery off the coast of California. Some of the trails exceed 1000 km in length and 20 km in width and they are evident in both the channel-4 infrared (IR, 11 μm) image (Fig. 2a) and in the image (Fig. 2b) of the 11-12 μm brightness temperature difference (T4-T5), a parameter that is used to differentiate contrails from cirrus clouds. The contrails in Figure 2 represent many different stages of growth and dissipation. Having lost

much of their distinct linearity, many of the older contrails are difficult to distinguish from natural cirrus clouds.

The automated algorithm of MANNSTEIN ET AL. (1999) was applied to the afternoon *NOAA-16* data taken over the domain bounded by 25° - 55°N and 120° - 150°W (Fig. 1) during May, August, and November 2002 and February 2003. These 4 months should be representative of the four seasons and provide an estimate of the annual mean contrail properties. PALIKONDA ET AL. (2004) discuss the application of the detection method. In this study, the domain was divided into 12 regions that were used separately for a given application of the methodology. Contrail visible optical depth was computed for each contrail pixel using the method of MEYER ET AL. (2002) assuming that the contrail temperature Tc is 224 K and that the contrail emissivity ε varies with optical depth (OD) for a given cosine of satellite viewing zenith angle, μ, according to the model of MINNIS ET AL. (1993) for small ice crystals:

$$\varepsilon = 1 - \exp[-0.458(OD / \mu)^{1.033}]. \quad (1)$$

The contrail emissivity is estimated as

$$\varepsilon = \{B(T4) - B(Tb)\} / \{B(Tc) - B(Tb)\}, \quad (2)$$

where B is the Planck function at 10.8 μm. The background brightness temperature Tb is computed as the mean value of the surrounding non-contrail pixels (PALIKONDA ET AL. 2004). Only pixels with a viewing zenith angle less than 50° are included the analysis because of an increase in false contrail detections with increasing viewing angles (PALIKONDA ET AL. 2002). Normalized contrail longwave radiative forcing (NCLRF) was computed using the methods of PALIKONDA ET AL. (2002, 2004). It cor-

responds to the longwave radiative forcing of contrail pixels only, i.e., 100% contrail coverage and is simply the difference between the outgoing longwave radiation (OLR) for a given area when no contrails are present and the OLR for the same area entirely covered by contrails. The contrail radiative forcing for all pixels in a given area is

$$\mathrm{CLRF} = \mathrm{NCLRF}\ Nc / N, \tag{3}$$

where Nc and N are the number of contrail and total pixels in a given area.

3 Results

Figure 3 shows the distribution of contrail coverage over the domain for the 4 months. The derived contrail coverage appears to be distributed relatively homogeneously during February (Fig. 3a) except for extremes of both signs over the western third of the domain. During May (Fig. 3b), the heavy coverage appears to be confined mainly to the coastal routes with some lesser amounts along the southwestern and western corridors. During August (Fig. 3c), the greatest contrail coverage occurred around 47°N, 142°W with a secondary maximum near the west-southwest approach to San Francisco. More coverage occurs in the northern part of domain, in general. Minimum coverage is seen in the southwestern corner of the domain, off the Oregon coast and inland. By November (Fig. 3d), the contrails occur primarily over the southern half of the domain and along the coastal routes. Overall, the observed mean contrail amounts were 0.67, 0.56, 0.51, and 0.51% during February, May, August and November, respectively.

The annual average distribution of contrail coverage (Fig. 4), based on the results in Figure 3, reveals that the persistent contrails were concentrated near the coast and west of northern California between 35°N and 42°N and along the coast and the northwestern corner of the domain. Contrails

were rarely detected along the southwest-to-northeast diagonal of the domain and off the southern California coast. The annual mean coverage between May 2002 and February 2003 is 0.56%. Figure 5 shows a histogram of the daily contrail coverage over the domain for the entire period. These results indicate that contrail-free days were rare and that on a given day, the contrail coverage was close to the average value. There appear to be more days when large outbreaks occur (values > 0.8%) than when few contrails are observed.

The frequency distributions of contrail *OD* and NCLRF are plotted in Figure 6. *OD* (Fig. 6a) varies according to a slightly skewed Gaussian distribution with a mode value around 0.30. Smaller values (*OD* < 0.20) are more common during February and May while thicker contrails (*OD* > 0.40) are more frequent during the summer and fall. The minimum and maximum mean ODs, 0.22 and 0.28, occur during May and November, respectively, bounding the annual mean of 0.26 (Table 1). The NCLRF distribution (Fig. 6b) is highly skewed with a mode near 8 Wm^{-2}. The smallest values are more common during winter and spring than during the rest of year. Conversely, NCLRF > 15 Wm^{-2} occurs more often during August and November. NCLRF ranges from 13.5 Wm^{-2} in February to 17.4 Wm^{-2} during August with an annual average of 15.2 Wm^{-2} (Table 1). The monthly mean CLRF only varies from 0.08 to 0.09 Wm^{-2} yielding an annual mean value of 0.085 Wm^{-2}. The variability in NCLRF arises from the large range in background radiating temperatures. Contrails mixed with other cirrus clouds will tend to have small values of NCLRF because the thermal contrast between the cirrus and contrails is small. Over clear areas, NCLRF will be much larger because the thermal contrast is greater than over clouds, especially over land during the afternoon.

4. Discussion

4.1 Accuracy of contrail detection

The automated detection method isolates linear features in the T4-T5 image and classifies the pixels comprising the lines as contrails if a predefined set of tests are met. The assumption of line-

arity can cause both under- and overestimates of contrail coverage. Contrails do not always maintain linearity causing the technique to miss some contrails. Natural clouds, rivers, and coastlines can also produce linear features that can be mistaken as contrails. The technique is also sensitive to background variations and to minor peculiarities in the relative calibrations of the AVHRR channels 4 and 5. Thus, it is essential to estimate the errors in the detection method for each satellite and region analyzed.

To effect the detection error analysis, a user-interactive computer program was developed to display the T4 and T4-T5 images with removable overlays of the automatically detected contrails. With the program, the analyst can evaluate the results both objectively by comparing T4 and T4-T5 values for the contrails with the surroundings and subjectively using contrast adjustment. Contrail pixels can be added or deleted based on the analyst's judgment. Deletions are made by selecting a rectangular box containing the false contrails and hitting the "delete" button. Additions are made for a selected box by setting T4 and T4-T5 thresholds to convert pixels having the encompassed values into contrail pixels. The thresholds are variable because the background values of T4 and T4-T5 can change significantly from one scene to the next. Thus, the thresholds are adjusted until the resulting contrail pixels are satisfactory to the analyst. Results are stored as images with the remaining, deleted, and added contrail pixels. The contrail properties can then be computed for all three categories.

Because the interactive analysis is labor intensive, only data for *NOAA-16* overpasses taken during 3 randomly selected days were analyzed for each month. Although this type of analysis is unavoidably subjective, the procedure follows some general guidelines. Among others, these include ensuring that the contrail is colder than the background and T4-T5 exceeds the background average, being aware of the air traffic corridors (contrails should not commonly occur with no air traffic), and assuming that contrails will generally not be oriented with the natural cirrus clouds (unless the air

traffic follows the orientation). Subjective analysis of the images is difficult especially when cirrus and contrails occur together. When it was not possible to decide if the pixels were actually contrails or cirrus, the automated result remained intact. The greatest overestimates generally occurred over the western portion of the domain as a result of cirrus streamers from cyclonic storms. Other common sources of overestimation are coastlines, rivers, cumulus streets, and cloud edges at high view angles. Underestimates generally occurred in contrail clusters, for older or faint contrails, and along the image edges because the method does not use the outer 10 pixels of the image. Pixels around the intersection of contrails were often missed. Although there was no attempt to explicitly add the cloudy pixels that were obviously from spreading contrails, some of those pixels were included in the additions because of variability in the required threshold for each contrail pixel. Conversely, some narrow contrails were not added for the same reason.

Figure 7 shows an example of the interactive error analysis program display (left panel) along with a T4 image (upper panel) taken west of California with the original contrails denoted in red, deleted contrails in blue, and added contrails in green. The corresponding T4-T5 image is shown in the lower panel. The top row of boxes in the display panel allow the user to set the thresholds. Image channels, overlays, and adding or deleting command buttons are available in the next rows. The user can also bound the range of T4-T5 and T4 values that are affected by the delete, add, or clean commands. Contrast for a given image is adjusted using the slide bars in the middle of the left panel, while file display commands are below the contrast slides. Finally, the image statistics window is shown at the bottom.

The contrails in the Figure 7 images are a mix of sharp, diffuse, and faint features, while some of the false contrails are edge features in the T4-T5 image (far right) or are judged to be streamers (middle right). These images reveal the difficulties of accurately determining what is and is not a contrail. Portions of the older diffuse contrails (lower right) are partially analyzed automatically (red) and

manually (green), but other parts are not included. The faint contrails classified as false returns in the middle of the image may or may not be contrails. The ambiguity is pervasive, especially when cirrus streamers occur as in Figure 8, which shows imagery for an area northwest of California. Contrast is enhanced in the T4 image (Fig. 8a) to show some of the cirrus streamer features that disappear to some extent in the T4-T5 image (Fig. 8b). Despite the lack of any sharp contrail-like features in the T4-T5 image, the algorithm classifies a fair number of the pixels as contrails that are deleted manually (blue). The few remaining contrails (red) are still somewhat ambiguous. The error analysis procedure is not ideal, but it should provide a more accurate assessment of the biases in the automated algorithm.

The results of the interactive analysis indicate that, relative to the number of detected contrail pixels, the method detected false contrails in 18 and 51% of the cases during May and February, respectively, with 29% for the other 2 months. On the other hand, 18% of the contrails were missed during May and February compared to 10 and 26% during November and August, respectively. Assuming that the results are representative of all of the analyzed images, it is possible to estimate correction factors to remove the biases. These factors, defined as the ratio of the number of deleted-to-original pixels multiplied by the ratio of the number of added-to-original contrail pixels, are 1.00, 0.96, 0.70, and 0.60 for May, August, November, and February, respectively. The resulting corrected monthly and annual mean contrail coverage amounts are listed in Table 1 along with the original values. After correction, the minimum contrail coverage shifted from November to February. The corrected annual mean for the *NOAA-16* overpass time is 0.45%, a value 20% less than the raw, observed average. If it is assumed that the errors are not dependent on location, then the geographical distribution of the corrected contrail coverage can be obtained by simply rescaling the color bars in Figures 3 and 4 by the correction factors in Table 1. Determining if that assumption is correct will require interactive analyses of a much larger dataset than used here.

Overall, contrail *OD* dropped somewhat when the false contrails were removed and the missed ones were added. The frequency distribution of the *OD*s for the error analysis dataset (Fig. 9a) shows that the deleted pixels tend to have slightly larger *OD*s than the remaining pixels and the added pixels are generally thinner than the original ones. The relative frequency of added pixels in the lowest *OD* category is twice that for the remaining and deleted pixels while the frequency of larger *OD*s is reduced. Overall, the *OD*s for the adjusted contrails are 2 - 8% less than those for the original dataset. The original and new *OD* histograms for the error analysis dataset are shown in Figure 9b, where the original frequencies are defined as the sum of the remaining and deleted pixels in each category divided by the total number of remaining and deleted pixels. The new frequencies are found in a similar manner using the remaining and added pixels. A correction factor, the ratio of new-to-old frequency, was computed for each category and used to adjust the histogram of ODs for the combined 4 months (annual) resulting in the new annual histogram. The corrected histogram of *OD*s plotted in Figure 9b shows the increase in thin cloud optical depths and decrease in thicker contrails relative to the annual mean. Figure 9b also confirms that the sampled error analysis dataset (denoted Original) is representative of the entire dataset.

Optical depth and NCLRF correction factors were derived from the error analysis dataset in the same manner used for contrail coverage and applied to the raw observations for each month. The corrected monthly and annual means given in Table 1 show that the *OD*s are still at a minimum in May and the corrected annual mean *OD* is 0.24. Table 1 includes the monthly and annual mean values of NCLRF. On average, NCLRF is reduced by 7% from 15.2 to 14.2 Wm^{-2}.

The original analysis did not include any pixels with $OD > 1$ as a means of eliminating some false positive detections. However, the error analysis, performed without the *OD* restriction, revealed that roughly 1 - 2% of the remaining and added pixels had $OD > 1$. Thus, the corrected means for all of the parameters in Table 1 are slightly underestimated by 1 - 2%. It should also be noted that the

determination of the background radiances used to compute *OD* and *NCLRF* can include pixels containing cirrus produced as a result of spreading contrails. In such cases, both *OD* and *NCLRF* will be underestimated.

4.2 Correction for diurnal cycle

An additional coverage correction is necessary because the afternoon *NOAA-16* sampling is not representative of the daily average air traffic over the Pacific. From the database of GARBER ET AL. (2004), it was determined that for the 3 hours straddling 2030 UTC, roughly 1 hour before *NOAA-16* passes over the center of the domain, the number of flights and cumulative flight length are 30% greater than the corresponding 24-hour means. Assuming that contrail formation conditions are independent of the time of day over a 1-month period, then the mean observed contrail coverage should be multiplied by 0.7. Thus, the best estimate of annual mean contrail coverage for the domain is 0.31% as shown in Table 1. Additional data from satellites with other overpass times should be analyzed to test the assumption of uniform conditions over the day.

4.3 Comparisons with model values and other observations

The diurnally corrected mean annual contrail coverage for the domain is very close to its theoretical counterpart of 0.30 (SAUSEN ET AL. 1998). If it is assumed that air traffic over the domain has increased by 2.5% per annum since 1992, the air-traffic year used by SAUSEN ET AL. (1998), and the contrail coverage increased by the same amount, then the theoretical coverage would be ~ 0.37%. Thus, the best estimate from the *NOAA-16* analysis agrees to within $\pm$20% with the theoretical contrail coverage. The theoretical calculations of PONATER ET AL. (2002) suggest that summertime contrail coverage over the area should be slightly larger than that during winter. The corrected current results agree in that the May and August means are 33% greater than the average for the other 2 months. From the error analysis, it was found that most of the false detections occurred over the western

portion of the grid where air traffic is minimal. Removal of those false contrails from Figure 4 would result in better agreement between the theoretical and observed contrail coverage distributions.

BAKAN ET AL. (1994) found a seasonal cycle in contrail coverage over the northeast Atlantic that is characterized by a summer maximum and an autumnal minimum that appear to be in phase with the movement of the polar jet stream. The relationship between contrails and the jet stream was further confirmed by DEGRAND ET AL. (2000), who found that nearly 80% of contrails observed over the USA were associated with baroclinic waves and the jet stream. The seasonal cycle in Figure 3 corresponds to only 4 months, so it cannot be related to the movement of the jet stream in a climatological sense. There appears to be some correspondence, however, between the coverage and jet stream for the months used here. During May, the jet stream was highly variable in orientation and location[2], which could explain the lack of a distinct pattern in Figure 3a. During August, the polar jet stream was weak and located mostly around 55°N. A sub-tropical jet developed during a few days in late August around 40°N. Contrails were more widespread in the northern part of the domain during August with some relative maxima occurred south of 40°N. During November, the jet stream was centered around 45°N and was more zonal than during the other months. Most of the contrail coverage during November was south of 45°N. Although some baroclinic waves travelled through the domain during February, the jet stream was often in an omega block centered near 130°W with south-to-north flow around 150°W and the subtropical jet to the south. The large coverage in Figure 3d around 45°N, 145°W is probably due to cirrus clouds and contrails associated with the southerly flow to the west. The appearance of more contrail coverage south or to the right of the jet stream flow in Figures 3b and 3c is consistent with the greater probability of cirrus formation at that position relative to the jet stream (MENZEL ET AL., 1992). More detailed analyses using individual images

[2]Jet stream data obtained from San Francisco State University Archived Jet Stream Analyses at http://squall.sfsu.edu/scripts/nhemjet_archloop.html.

and synoptic maps or monthly averages of contrail coverage are needed to conclusively relate the contrail coverage and jet stream location during the May and February. Nevertheless, the differences between the phase in the contrail seasonal cycles over the northeast Atlantic and Pacific are probably closely related to differences in the intensity and movement of the jet streams in those two areas.

The contrail optical depth distributions and mean values are nearly identical to those derived over the USA by PALIKONDA ET AL. (2004). The means are more than twice the magnitude found over Europe by MEYER ET AL. (2002) and 67% greater than the global average estimated by PONATER ET AL. (2002) from theoretical calculations. Although the differences could be related to misclassified cirrus clouds that are deeper than the average contrail, this explanation is unlikely given that the error analysis showed that the current *OD* values are fairly robust. The smaller observed values over Europe may be due to reduced supersaturations available for contrail growth while the theoretical calculations may underestimate *OD* in parts of the globe.

The February *NCLRF* mean is 5 Wm^{-2} greater than the wintertime mean for *NOAA-16* results over the USA while the August *NCLRF* is 2 Wm^{-2} less than the corresponding USA summertime mean (PALIKONDA ET AL. 2004). This seasonal difference in NCLRF is likely due to the relatively stable background temperatures over the ocean. Over land, the contrast between the contrail and surface temperatures is much greater in summer than in winter. The mean value of *NCLRF* is nearly identical to the normalized *net* radiative forcing computed for the zone between 25°N and 55°N from the data of MINNIS ET AL. (1999) by scaling the results for $OD = 0.25$. Assuming that the ratio of the longwave-to-net forcing computed from the results in Table 1 of MINNIS ET AL. (1999) for $OD = 0.3$ holds for any location, the *NCLRF* from that earlier study would be ~23 Wm^{-2} or 60% greater than the value seen here. It is not clear, however, that the Northeast Pacific domain is representative of the entire latitudinal band. If it is, then it is likely that the observed contrails occur more fre-

quently over high clouds than assumed by MINNIS ET AL. (1999). Presumably, the NCLRF from PONATER ET AL. (2002) would be considerably smaller than that computed here because the global mean from that study is roughly an order of magnitude smaller than that from MINNIS ET AL. (1999).

5 Concluding remarks

The results presented here constitute the first objective analysis of linear contrails over the eastern North Pacific. After correction for errors, the contrail coverage is in good agreement with the amount derived theoretically. However, the corrected optical depths are twice as large as those derived over Europe from satellite data and from theoretical calculations. Contrail longwave radiative forcing appears to be much greater than that computed theoretically. Further study is required to understand the various discrepancies. Nevertheless, the results provide another point of validation for the global estimation of contrail coverage.

Future studies of contrails over this area should also compute the shortwave radiative forcing to obtain the net forcing by contrails. Shortwave forcing is more difficult to estimate because of the greater impact of the diurnal cycle on the relative albedos of the contrail and the underlying background. To better understand diurnal and interannual variability in contrail properties, additional analyses should be performed including data from other NOAA satellites and the NASA *Terra* and *Aqua* satellites to improve diurnal coverage. Error analyses that pinpoint the locations of false detections should also be undertaken to facilitate further comparisons of model and satellite-derived parameters. The new tool developed for interactive contrail analysis may also prove valuable for measuring the extent of contrail spreading, thus providing a more comprehensive assessment of the impact of contrails on climate. The results of this study will be compared with the model-predicted temperature and humidity conditions to help improve the parameterization of contrails in climate

models so that a more accurate assessment of contrail effects can be computed for the Northeastern Pacific Ocean.

Acknowledgments

This research was supported by the NASA Pathfinder Program and the NASA Office of Earth Science Radiation Sciences Program. The original air traffic summary was provided by Don Garber. We thank Dr. Klaus Gierens for providing the theoretical 1992 contrail coverage database.

References

DEGRAND, J. Q., A. M. CARLETON, D. J. TRAVIS, and P. J. LAMB, 2000: A satellite-based climatic description of jet aircraft contrails and associations with atmospheric conditions, 1977-79. - J. Appl. Meteorol., **39**, 1434-1459.

GARBER, D. P., P. MINNIS, and P. K. COSTULIS, 2004: A USA commercial flight track database for upper tropospheric aircraft emission studies. - Meteorol. Z., submitted.

MANNSTEIN, H., R. MEYER, and P. WENDLING, 1999: Operational detection of contrails from NOAA AVHRR data. - Int. J. Remote Sens., **20**, 1641-1660.

MENZEL, W. P., D. P. WYLIE, and K. I. STRABALA, 1992: Seasonal and diurnal changes in cirrus clouds as seen in four years of observations with the VAS. - J. Appl. Meteorol., **31**, 370-385.

MEYER, R., H. MANNSTEIN, R. MEERKÖTTER, U. SCHUMANN, and P. WENDLING, 2002: Regional radiative forcing by line-shaped contrails derived from satellite data. - J. Geophys. Res., **107**, D10 10.1029/2001JD000426.

MINNIS, P., J.K. AYERS, R. PALIKONDA, and D. PHAN, 2004: Contrails, cirrus trends, and climate. - J. Climate, **17**, 1671-1685.

MINNIS, P., U. SCHUMANN, D. R. DOELLING, K. M. GIERENS, and D. FAHEY, 1999: Global distribution of contrail radiative forcing. - Geophys. Res. Lett., **26**, 1853-1856.

MINNIS, P., Y. TAKANO, and K.-N. LIOU, 1993.: Inference of cirrus cloud properties using satellite-observed visible and infrared radiances, Part I: Parameterization of radiance fields. - J. Atmos. Sci., **50**, 1279-1304.

PALIKONDA, R., P. MINNIS, P. K. COSTULIS, and D. P. DUDA, 2002: Contrail climatology over the USA from MODIS and AVHRR data. *Proc. 10th Conf. on Aviation, Range, and Aerospace Meteorology*, Portland, OR, May 13-16, J9-J12.

PALIKONDA, R., P. MINNIS, D. R. DOELLING, P. W. HECK, D. P. DUDA, H. MANNSTEIN, and U. SCHUMANN: Potential radiative impact of contrail coverage over continental USA estimated from AVHRR data. *Proc. AMS 10th Conf. Atmos. Rad.*, Madison, WI, June 28 – July 2, 181-184.

PALIKONDA, R., P. MINNIS, D. P. DUDA, and D. N. PHAN, 2004: Contrail coverage over the USA from AVHRR data. - Meteorol. Z., accepted.

PONATER, M., S. MARQUART, and R. SAUSEN, 2002: Contrails in a comprehensive global climate model: parameterisation and radiative forcing results. - J. Geophys. Res., **107**, 10.1029/2001JD000429.

SAUSEN, R., K. GIERENS, M. PONATER, M. and U. SCHUMANN, 1998: A diagnostic study of the global coverage by contrails, part I, present day climate. - Theor. Appl. Climatol. **61**, 127-141.

ZEREFOS, C. S., K. ELEFTHERATOS, D. S. BALIS, P. ZANIS, G. TSELIOUDIS, and C. MELETI, 2003: Evidence of impact of aviation on cirrus cloud formation. – Atmos. Chem. Phys., **3**, 1633 – 1644.

Table 1. Summary of contrail properties for North Pacific domain (25°N - 55°N, 120°W - 150°W) during May 2002 - February 2003.

	Contrail Coverage (%)			Optical Depth		NCLRF (Wm^{-2})	
	observed	corrected	diurnally adjusted	observed	corrected	observed	corrected
May	0.56	0.56	0.39	0.22	0.20	13.9	13.5
August	0.51	0.49	0.34	0.26	0.26	17.4	15.8
November	0.51	0.36	0.25	0.28	0.26	16.1	15.3
February	0.67	0.40	0.28	0.27	0.24	13.5	12.3
Annual	0.56	0.45	0.31	0.26	0.24	15.2	14.2

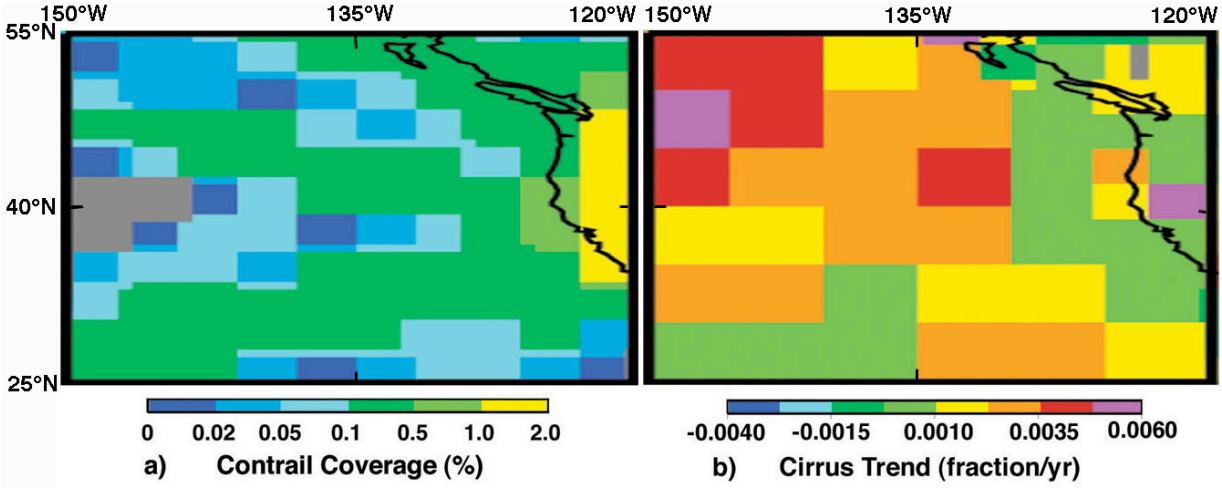

Figure 1: Theoretical linear contrail coverage in 1992 (a) and trend in surface-observed 1971-1996 cirrus coverage (b).

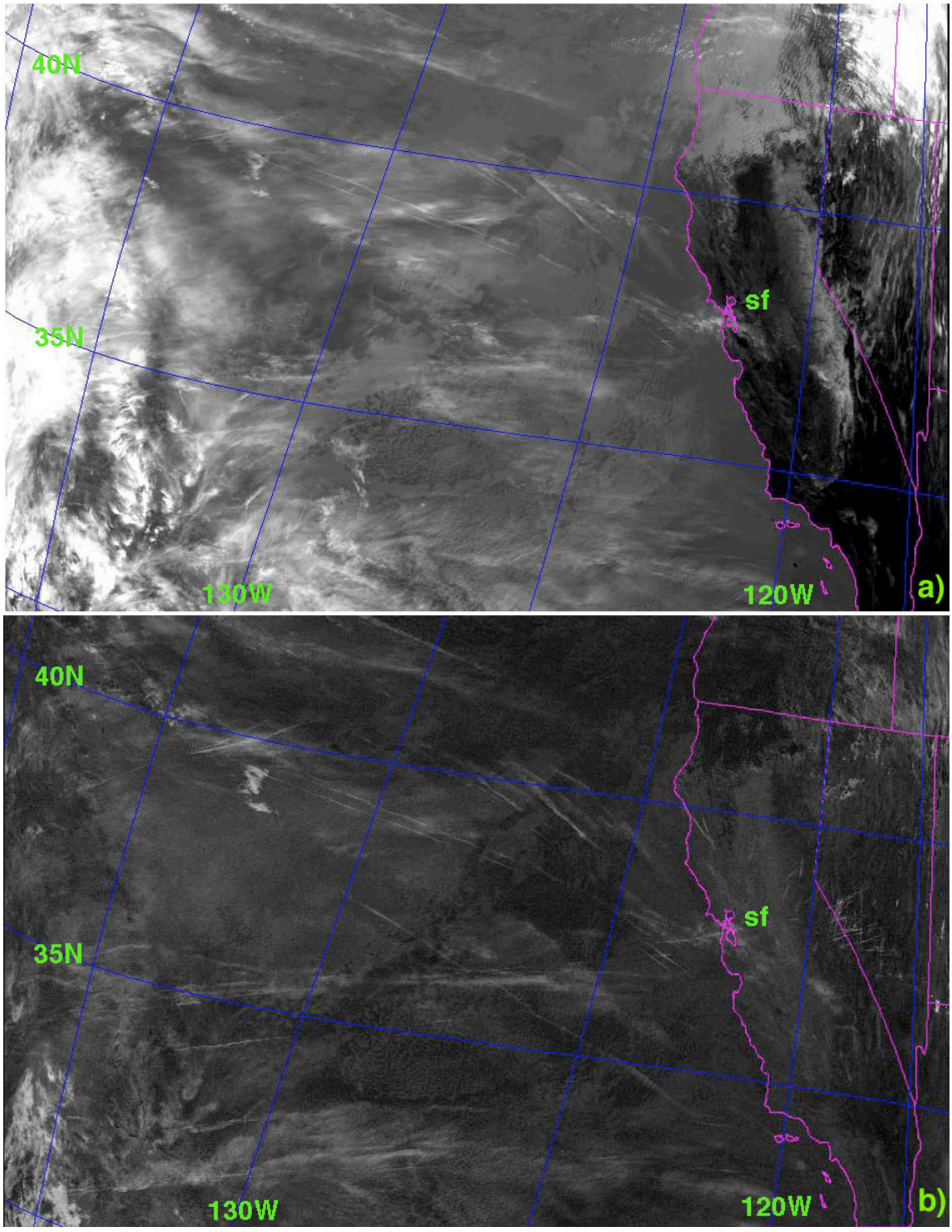

Figure 2: *NOAA-16* AVHRR imagery at 2100 UTC, 21 February 2003: (a) Infrared brightness temperature and (b) channel 4-5 brightness temperature difference. Proximity of San Francisco, CA is indicated by "sf"

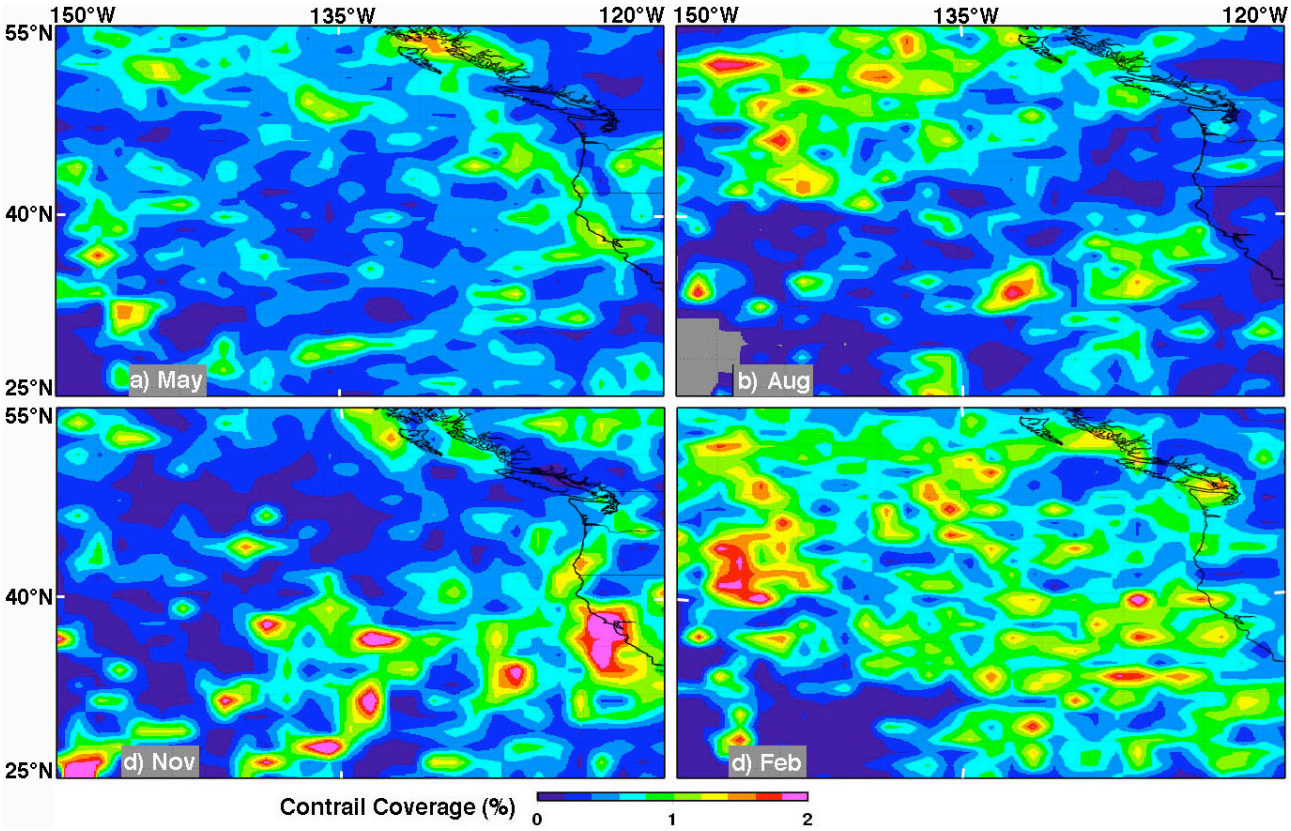

Figure 3: Monthly mean contrail coverage derived from afternoon (1430 LT) *NOAA-16* AVHRR data during (a-c) May, August, and November, 2002 and (d) February 2003.

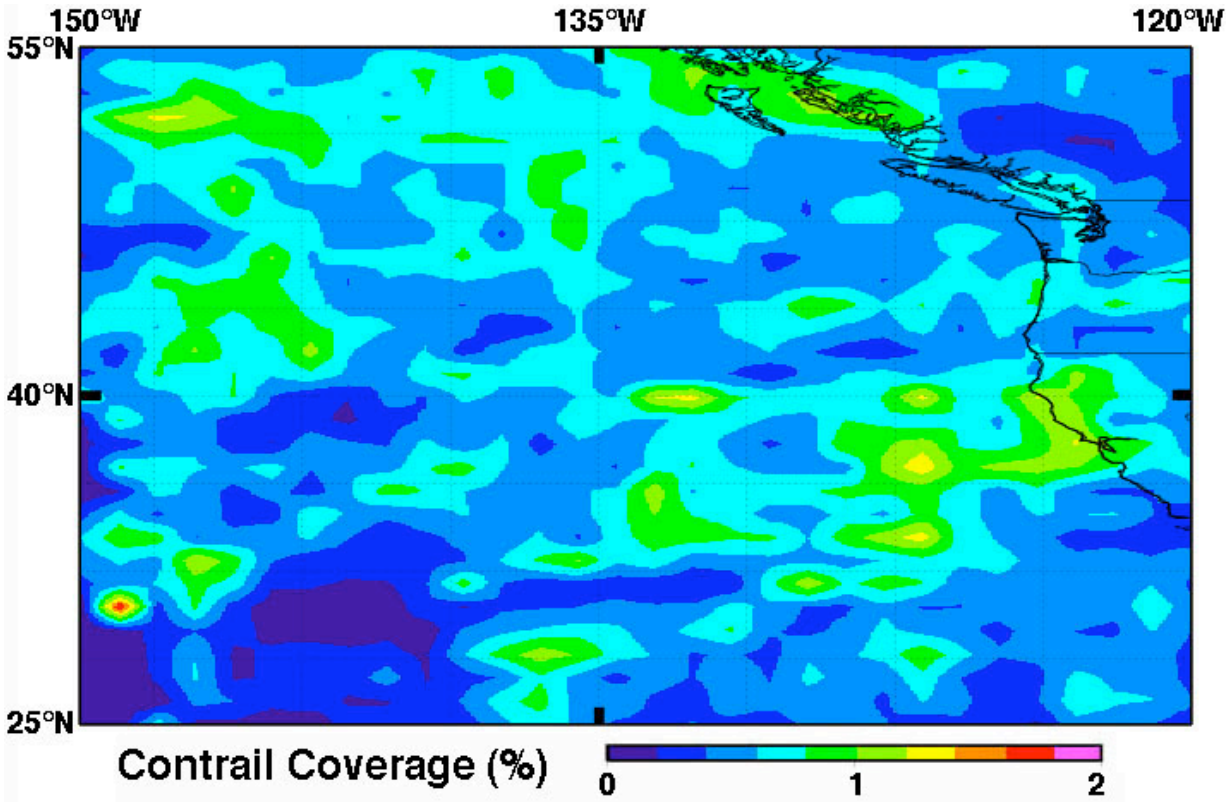

Figure 4: Monthly mean contrail coverage derived from afternoon (1430 LT) *NOAA-16* AVHRR data during 2002 (b-d) and 2003 (a).

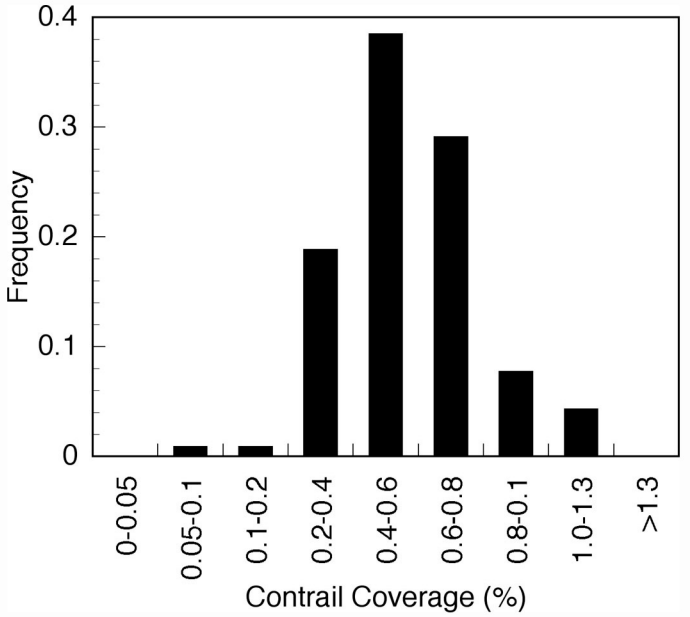

Figure 5: Histogram of daily domain contrail coverage for all 4 months.

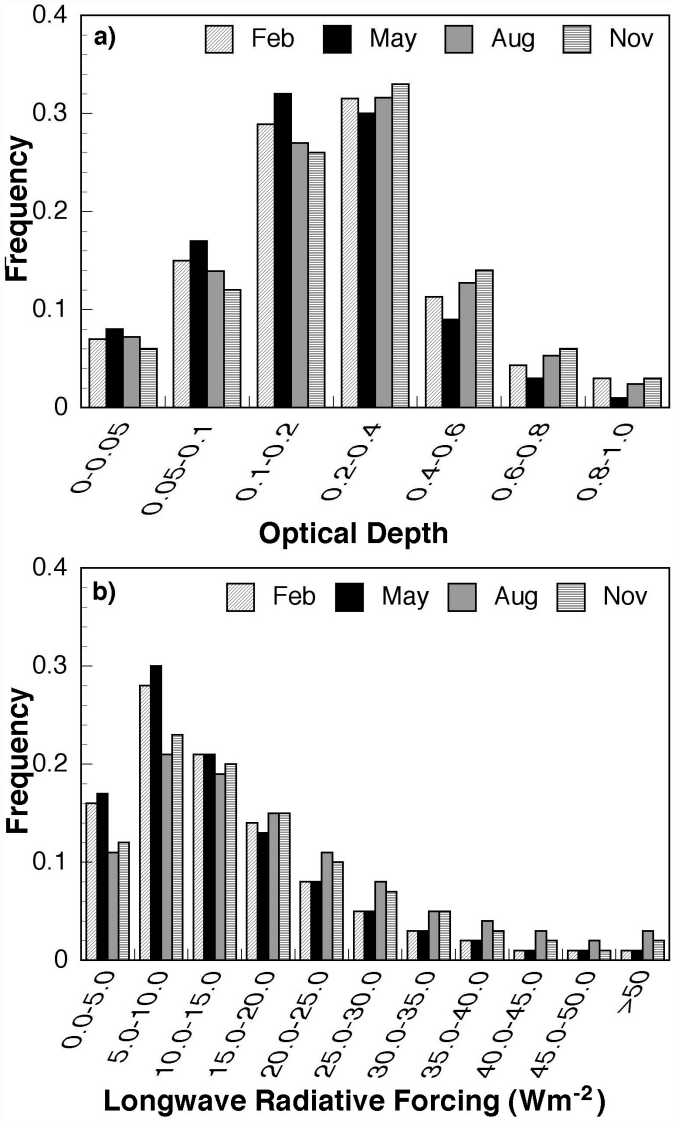

Figure 6: Frequency distributions of (a) contrail optical depth and (b) NCLRF during May 2002 - February 2003.

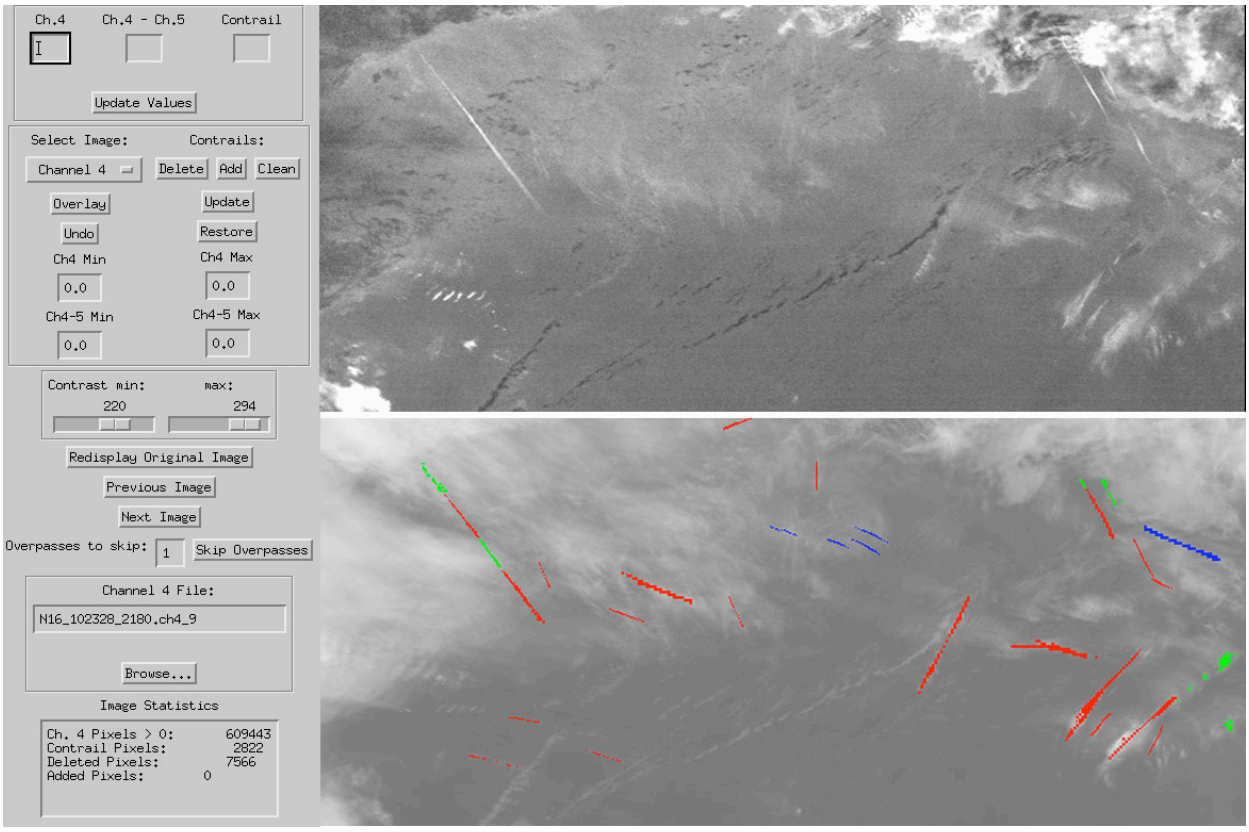

Figure 7: Error analysis display (left panel) with superimposed NOAA-16 AVHRR T4-T5 image (top) and T4 image taken over the northeastern Pacific at 21.92 UTC, 14 November 2002 with contrail pixels indicated in color: original (red), deleted (blue), and added (green).

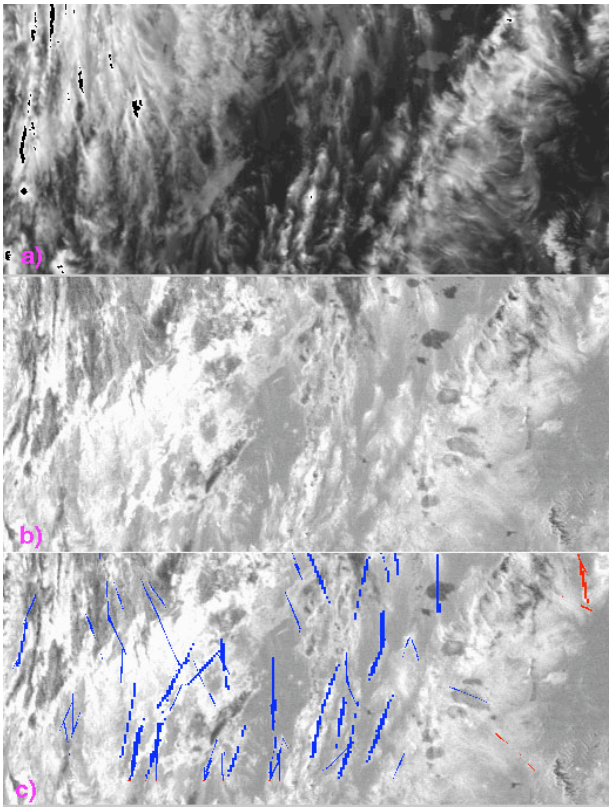

Figure 8: Contrail error analysis example for NOAA-16 AVHRR imagery taken over northeastern Pacific at 21.80 UTC, 24 November 2002. (a) Contrast enhanced T4, (b) T4-T5, (c) T4-T5 with original (red) and deleted (blue) contrail pixel overlay.

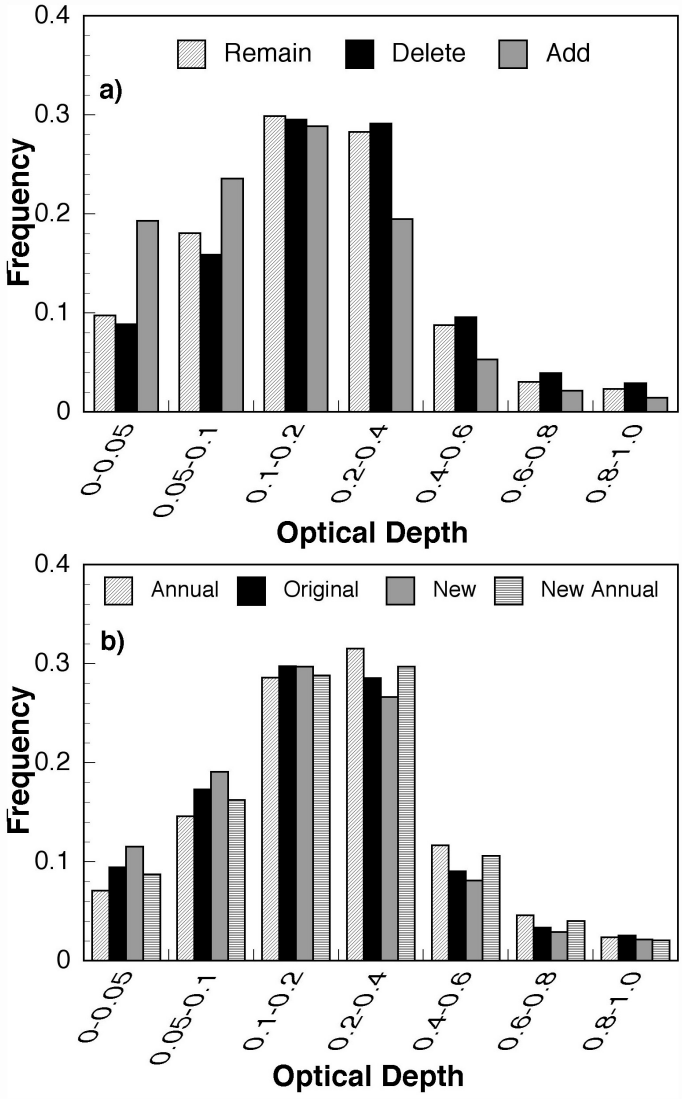

Figure 9: Frequency distributions of contrail optical depths for (a) error analysis dataset and (b) domain annual mean (annual) and corrected annual mean (new annual) and original error analysis dataset (re-maining + deleted = original) and corrected error analysis dataset (remaining + added = new).